Chemical Physics Letters 646 (2016) 6–11

Contents lists available at ScienceDirect

Chemical Physics Letters

journal homepage: www.elsevier.com/locate/cplett

Electron density profile at the interfaces of bulk heterojunction solar cells and its implication on the S-kink characteristics

Abhay Gusain[a], Surendra Singh[b], A.K. Chauhan[a], Vibha Saxena[a,*], P. Jha[a], P. Veerender[a], Ajay Singh[a], P.V. Varde[c], Saibal Basu[b], D.K. Aswal[a,*], S.K. Gupta[a]

[a] Technical Physics Division, Bhabha Atomic Research Center, Mumbai 400085, India
[b] Solid State Physics Division, Bhabha Atomic Research Center, Mumbai 400085, India
[c] Research Reactor Services Division, Bhabha Atomic Research Center, Mumbai 400085, India

ARTICLE INFO

Article history:
Received 14 October 2015
In final form 25 December 2015
Available online 31 December 2015

ABSTRACT

The efficiency of a bulk heterojunction (BHJ) solar cell critically depends upon quality of its interfaces. The imperfect interfaces can lead to S-kink in the current–voltage characteristics that reduce the efficiency of BHJ solar cells. In this letter, using PCDTBT:PCBM based BHJ solar cells, we demonstrate that non-destructive X-ray reflectivity is powerful technique to estimate the electron density profile across the BHJ solar cells. A direct correlation is observed between the enhanced electron density at PEDOT:PSS/PCDTBT:PCBM interface and appearance of S-kink in *J–V* characteristics, which is also supported by X-ray photoelectron spectroscopy and Kelvin probe measurements.

1. Introduction

Organic bulk heterojunction (BHJ) solar cells are potential candidate for applications due to several advantageous factors, including low weight, flexibility, lower manufacturing costs, easier integration with other products, low environmental impact during manufacturing and operations and short energy payback times [1–3]. BHJ solar cell consists of a blended donor–acceptor active layer, e.g. poly(3-hexylthiophene) (P3HT) and phenyl C_{61}-butyricmethyl ester (PCBM), etc., which is sandwiched between a hole-collecting anode (e.g. PEDOT-PSS/ITO) and an electron-collecting cathode (e.g. Au, Al, etc.). The built-in voltage (V_{bi}) drives photo-generated holes to anode and electrons to cathode. The efficiency of BHJ solar cell is directly associated with the current–voltage (*J–V*) characteristics under illumination, which is governed by the quality of various layers and interfaces involved in devices. However, in some cases instead of diode-like *J–V* characteristics under 1 sun, S-shaped characteristics are observed i.e. with increasing bias voltage, current levels off and again increases as voltage approaches to open circuit voltage (V_{OC}). The observation of S-kink in the *J–V* characteristics leads to decrease in fill factor (FF), V_{OC} and, in turn the lowering of overall device efficiency. Generally, the S-kink is observed due to following reasons:

(i) *Injection and extraction barriers*: The injection and extraction barriers across the hole transport layer (HTL)/donor interface can arise either due to mismatched electrode work functions or presence of interface defects and traps. Shaheen et al. studied the effect of several cathode materials such as Al, Ag, Mg:Ag/Ag, LiF/Al, Ca/Al, and Ba/Al on the device efficiency and stability [4]. They observed S-kink in low work function cathode material. Tress et al. suggested that V_{OC} does not get affected by the extraction barrier but reduces in case of injection barrier. When the barrier exceeds 0.2 eV, S-kink is observed [5]. Wagenpfahl et al. suggested that the injection barrier changes the charge-carrier density at the contacts and therefore affects the V_{OC} [6]. However, numerical device simulation attributed the appearance of S-kink in case of reduced surface recombination velocity occurring in the device. By choosing an hole injection layer with high work function or doped buffer layers, the energetic barrier between donor and anode can be reduced resulting in normal device characteristics [7,8]. Similarly, the choice of bathocuproine (BCP) as an exciton blocking layer (EBL) or resulted in elimination of S-shape as a result of improved charge extraction [9].

(ii) *Interface dipoles*: The presence of defects and traps can result in interfacial dipoles causing barrier formation for carrier

* Corresponding authors.
E-mail addresses: vibhas@barc.gov.in (V. Saxena), dkaswal@yahoo.com (D.K. Aswal).

http://dx.doi.org/10.1016/j.cplett.2015.12.055
0009-2614/

extraction [10]. It is observed by Hany et al. that isolated Al clusters formed during cathode evaporation lead to defect states close to interface and thereby change the electric field distribution in the device [11]. The presence of strong interfacial dipoles results in the charge blockage, leading to an S-kink in *J–V* characteristics of device under illumination.

(iii) *Unbalanced mobility of charge carriers*: Unbalanced mobility of hole and electrons results in accumulation of charge carriers of lower mobility at the electrode surface causing an additional electric field in the device. Riede et al. carried out electrical simulation based on drift-diffusion model and predicted that the S-kink is observed if mobility mismatch factor is larger than 100 [12]. The theory was verified by combining low mobility material with acceptor having different electron mobilities. S-kink has also been eliminated by improving the hole mobility of donor material [13].

(iv) *Interfacial morphology*: Interfacial morphology of the donor/acceptor blends also causes S-shape in the *J–V* characteristics due to oxygen doping during processing or ambient air operation [5]. An efficient device operation for normal structure requires vertical phase separation of donor and acceptor at anode and cathode, respectively. It was found that fullerene localization at the anode interface leads to S-kink [14]. Further, the morphology also varied depending upon the processing using a mixture of solvents. Low surface energy of P3HT results in a thin P3HT enriched layer on top surface causing the S-kink. Usage of high boiling point solvent such as p-xylene suppresses the P3HT enrichment and thereby eliminating the S-kink [15].

It is to be noted that though there may be several reasons for the appearance of S-kink in the *J–V* characteristics, the effect remains the same i.e. charge accumulation in the device leading to additional electric field and therefore reduced FF and device efficiency. In order to identify the causes of the S-shaped *J–V* characteristics, measurements have been carried out either as a function of temperature/light intensity or transient photocurrent measurements, which reveal redistribution of the electric field [16,17]. Earlier we have shown that BHJ devices based on poly[[9-(1-octylnonyl)-9H carbazole-2,7-diyl]-2,5 thiophenediyl-2,1,3-benzothiadiazole-4,7-diyl-2,5 thio phenediyl] (PCDTBT) and PCBM exhibit S-kink when annealed at moderate temperatures of 100 °C for few hours [18] and similar results have recently been obtained by others [19]. The spectroscopic studies have shown that the properties of the PCDTBT:PCBM active layer almost remained unaffected at such low annealing temperatures [18], and hence, the appearance of S-kink could be associated with the degradation of interfaces. Therefore, a robust characterization technique, preferably using a nondestructive technique, is required to prepare high-quality BHJ solar cells so that the key physical parameters, such as, layer thickness, interfacial quality and density are well controlled. In addition, high efficient tandem BHJ solar cells require a proper nondestructive tool to characterize various layers and interfaces beforehand.

X-ray reflectivity (XRR) is an efficient and powerful nondestructive technique for the measurements of layer thickness, surface roughness and electron density profile in multilayers [20,21], and therefore, is suitable for investigating the origin of S-kink in BHJ solar cells. In this letter, for the first time, we investigate the PCDTBT:PCBM based BHJ solar cells using XRR and demonstrate a correlation between the electron density at the interface and presence of S-kink in the *J–V* characteristics. This correlation has further been supported using X-ray photoelectron spectroscopy (XPS) and Kelvin probe (KP) measurements.

2. Experimental

ITO-coated (resistivity: 8–12 Ω/sq) glass slides were first cleaned with detergent, ultrasonicated in deionized water, acetone and isopropyl alcohol for 15 min each followed by an ozone treatment for 20 min. In different experiments, 70 nm thick layer of PEDOT:PSS (obtained from Ossila® and filtered through 0.45 μm PTFE filter) was spin-coated onto ITO substrates. These samples were then transferred to glove box (MB 200G, MBraun Inc. Germany) having moisture and oxygen <0.1 ppm and annealed at 130° for 30 min. The active layer (thickness: 70 nm) of PCDTBT:PCBM (1:4 W/W, 10 mg/ml in 1,2-dichlorobenzene) was spin-coated on the PEDOT:PSS/ITO anodes. Finally, Al cathode (thickness: 100 nm) was thermally evaporated through a shadow mask on active layer to obtain BHJ solar cells with an active area of 4 mm^2. These solar cells were encapsulated using UV curable epoxy inside the glove box and taken out for photovoltaic characterization. More than 100 devices were fabricated and characterized. The current–voltage (*J–V*) characteristics of the devices were measured using a solar simulator (Sciencetech, Canada) under 1 sun (AM 1.5 G), 100 mW/cm^2 illumination. The intensity was calibrated using a standard silicon reference diode. A non-contact, non-destructive vibrating capacitor device, known as Kelvin probe (KP) scanning microscopy, was employed to measure the work function of PEDOT:PSS surface having resolution of ~0.003 eV (model: KP Technology). XPS was carried out using Mg Kα source (RIBER MBE system). The binding energy scale was calibrated to the Au $4f_{7/2}$ line of 83.95 eV. X-ray reflectivity (XRR) measurements were carried out using 18 kW rotating anode X-ray laboratory source with Cu Kα-radiation (wavelength, λ = 1.542 Å).

3. Results and discussion

Majority of the fabricated PCDTBT:PCBM BHJ solar cells exhibited nice diode-like *J–V* characteristics under the illumination of 1 sun (Figure 1(a)), whereas ~20% of them exhibited S-kink in their *J–V* characteristics (Figure 1(b)). The photovoltaic parameters of these devices are summarized in Table 1. Devices without S-kinks exhibited efficiency in the range of 2.1–3.1%, whereas the devices with S-kinks exhibited poor efficiency (0.5–1.3%) owing to poor V_{OC}, current density (J_{SC}) and FF. It is to be noted that devices were fabricated with basic cell design without any kind of post or pre-treatment as well as buffer layers in order to identify the cause

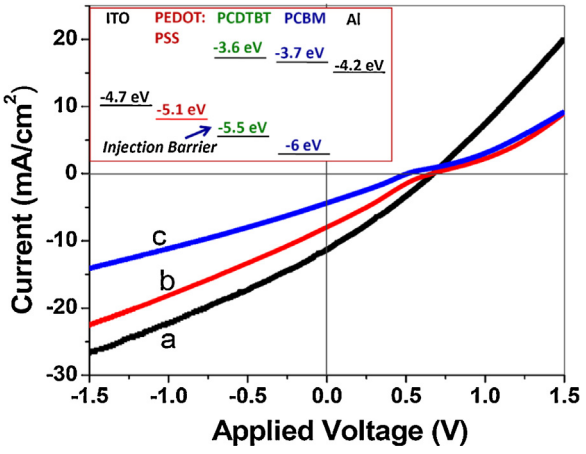

Figure 1. Typical experimental *J–V* curves recorded for devices under 1 sun (AM 1.5 G), 100 mW/cm^2 illumination for (a) devices without S-kink, (b) devices with S-kink and (c) appearance of S-kink after annealing (100 °C for 4 h) the devices representing (a). The inset shows energy levels of the materials employed in the device fabrication, and represents injection barrier for holes.

Table 1
Summary of photovoltaic parameters of different BHJ solar cells and estimated parameters of the (PCDTBT:PCBM)/(PEDOT:PSS) interface using XRR measurements.

BHJ solar cell	Photovoltaic parameters				Parameters of PCDTBT:PCBM/PEDOT:PSS interface		
	V_{OC} (V)	J_{SC} (mA/cm^2)	FF (%)	η (%)	Thickness (nm)	Electron density (e/nm^3)	Roughness (nm)
Without S-kink	0.52–0.67	11.3–15.5	28–39	2.1–3.1	7.5 ± 0.5	50 ± 15	1.2 ± 0.3
With S-kink	0.41–0.66	4.1–8	25–30	0.5–1.3	8.5 ± 0.3	874 ± 24	1.0 ± 0.2
Annealed@100 °C/4 h	0.51–0.52	4.5–12.2	27–34	0.6–2.1	7.5 ± 0.5	189 ± 15	1.4 ± 0.2
Annealed@100 °C/8 h	0.49–0.54	4.5–8.4	22–34	0.6–1.1	8.0 ± 0.5	370 ± 16	2.4 ± 0.2
Annealed@100 °C/16 h	0.45–0.50	5.6–6.1	22–30	0.4–0.8	8.5 ± 0.5	359 ± 17	4.5 ± 0.3
Annealed@100 °C/20 h	0.40–0.42	3.6–4.9	18.2–25	0.5–0.6	8.5 ± 0.5	349 ± 18	4.5 ± 0.2

of S-kink. In literature, the efficiency of PCDTBT:PCBM BHJ solar cells is found to depend upon several factors, including molecular weight of the donor material, pre- and/or post-treatments, thickness of active layer, buffer layers, device structure, etc. [19,22–24]. The best efficiency of ~3.1% observed in our case is comparable to the efficiencies reported for PCDTBT:PCBM BHJ solar cells fabricated under identical processing conditions [25–27]. However, the efficiency can be further improved to ~5% if one employs appropriate buffer layers and solvent/thermal treatments. The main purpose of this work is to investigate why some of the BHJ solar cells (fabricated under identical conditions), exhibit S-kink. Therefore, we have neither added buffer layer nor subjected the devices for any kind of treatments as it would lead to additional parameters for the investigations.

One of the possibilities envisaged for the observation of S-kink in some of the devices was if the quality of deposited PEDOT:PSS layer is varying from sample to sample, which in turn may lead to a poor quality of (PCDTBT:PCBM)/(PEDOT:PSS) interface. To investigate the role of PEDOT:PSS layer on the S-kink, the work function of several freshly-prepared PEDOT:PSS samples were measured using Kelvin probe method. As shown in Figure 2, it was found that though majority of PEDOT:PSS layers have an average work function of 5.1 eV (Figure 2(a)), few of them exhibited an average work function of 5.3 eV (see Figure 2(b)) that is significantly higher by 0.2 eV. The values obtained using this method may be different from those obtained from ultraviolet photoelectron spectroscopy (UPS) since KP gives an average value over a sample while UPS is a localized measurement [28]. The increase in the work function of the PEDOT:PSS may be associated with the presence of surface states or dipoles which might be created either due to chemisorbed oxygen or excess PSS at the surface. It has been reported that the charges of $PEDOT^+$ and PSS^- cause formation of local dipoles [29]. The orientation of these dipoles with sulphate groups toward surface leads to an increase in the work function. Therefore, an increase in the work function of PEDOT:PSS films could be due to the top layer of PEDOT:PSS which may contain excess of PSS owing to thermal treatment. Other reason for the increment in the work function may be due to chemisorbed oxygen. The work function of PEDOT:PSS affects the energy barrier height at the interface of PEDOT:PSS with the active layer as shown in inset Figure 1, and therefore, determines the hole injection at this interface leading to S-kink observed in *J–V* characteristics.

In order to further investigate why some of the PEDOT:PSS layers exhibit higher work functions, core level S2p and O1s XPS spectra were recorded for PEDOT:PSS layers exhibiting different work functions (Figure 3). The low binding energy peak corresponds to S atoms in the thiophene ring while high binding energy peak is attributable to sulphur atoms in PSS [30]. A single spin-orbit doublet having ratio of $2p_{3/2}$ and $2p_{1/2}$ ~ 2:1 and splitting of 1.2 eV was used for all deconvolutions. A doublet at 169.7 eV (S $2p_{3/2}$) and 168.5 eV (S $2p_{1/2}$) was attributable to PSSH, and that at 165.9 (S $2p_{3/2}$) and 164.5 (S $2p_{1/2}$) was assigned to sulphur of PEDOT. As shown in Figure 3(a) and (b), the S 2p spectra were found to be identical for all the samples with PSS/PEDOT ratio of 1:2.5, confirming that there is no loss or degradation of the material. However, the O1s spectrum of PEDOT:PSS layer having higher work function exhibited a broader and asymmetric peak as shown in Figure 3(c) and (d). In the case of PEDOT:PSS layer with lower work function (i.e. 5.1 eV), the O1s spectrum could be deconvoluted into oxygen component corresponding to various bonds in PEDOT:PSS i.e. 534.1 eV from the oxygen atoms in the dioxyethylene bridge of PEDOT (O_{PEDOT}), and 533 eV and 532.2 eV from the oxygen atoms bound to the sulfur sites in the sulfonic acid groups of PSS (O_{PSS}) [31]. The peak at 531.7 eV is attributed to the presence of physisorbed oxygen in PEDOT:PSS films, which is due to the fact that the films got exposed to ambient during their loading into XPS chamber. The PEDOT:PSS ratio as derived from the O_{PEDOT}:O_{PSS} ratio is found to be 1:2.5, which is consistent with the ratio estimated from S 2p data. In the case of PEDOT:PSS layers with higher work function, the ratio O_{PEDOT}:O_{PSS} is increased to 1:3. It is seen from the deconvoluted curves that relative intensity of the peak at 532.3 eV corresponding to PSS is enhanced significantly as

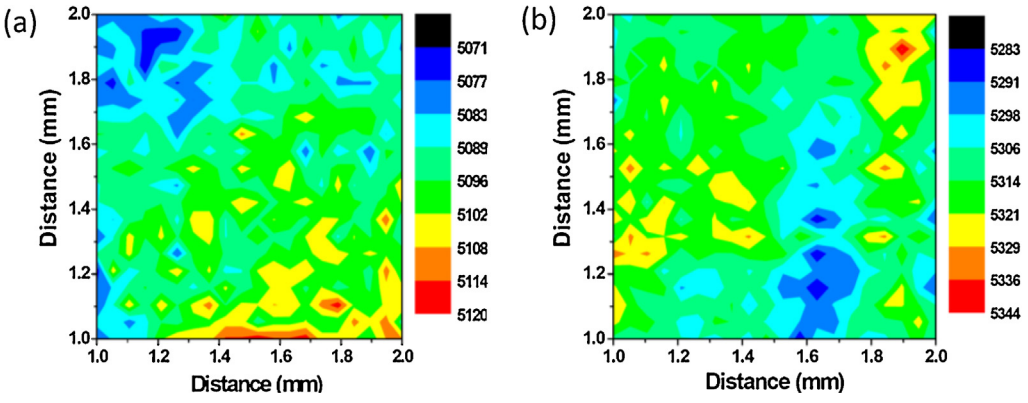

Figure 2. Work function mapping of PEDOT:PSS layers recorded using Kelvin probe exhibiting average work function value of (a) 5.1 eV and (b) 5.3 eV.

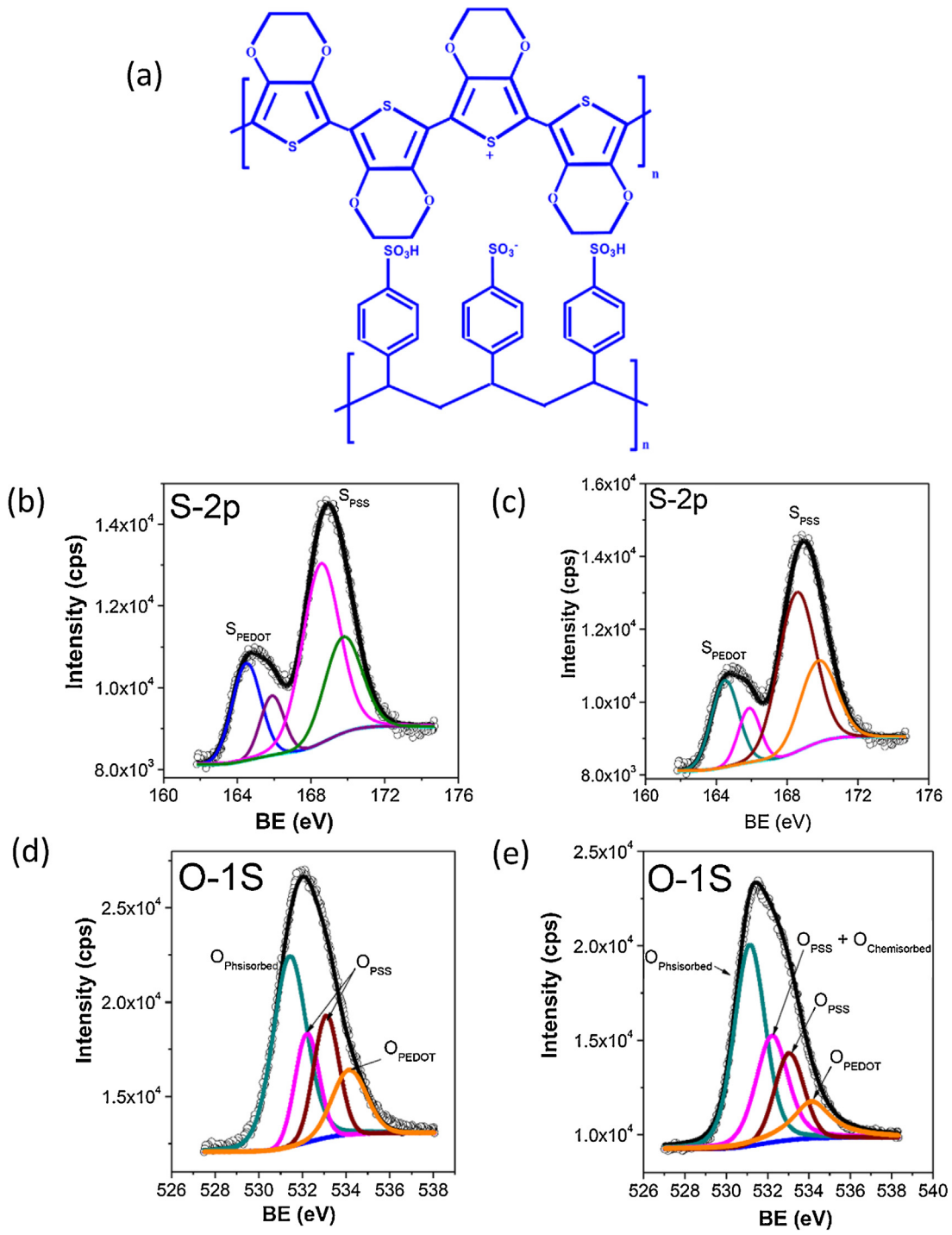

Figure 3. (a) Structure of PEDOT:PSS and (b) S2p and O1s XPS spectra of the PEDOT:PSS samples (b) and (d), and (c) and (e) corresponding to average work function value of (a) 5.1 eV and (b) 5.3 eV for the samples, respectively.

compared to the other component of PSS. The enhanced intensity at 532.3 eV can arise due to the presence of chemisorbed oxygen in PEDOT:PSS sample which overlaps with the peak of PSS. The presence of chemisorbed oxygen is attributed to the possible reaction of PEDOT:PSS with molecular oxygen and/or water. It has been known that even small amounts of water in the anode results in deterioration of device properties [32,33]. PEDOT/PSS in air contains a significant amount of water because of the hydroscopic properties of PSS. In fact this effect was predominantly observed, when PEDOT:PSS film was subject to an UV–ozone treatment [34]. It is therefore anticipated that due to slight unintended variations in the processing conditions (e.g. concentration of solution, extra exposure to the ambient, etc.) chemisorbed oxygen can be present at the PEDOT:PSS surface, which could be the responsible factor for observed S-kink in the devices. It may further be noted that devices exhibiting nice diode-like *J–V* characteristics started showing S-kink when they were annealed at 100 °C for more than 4 h (Figure 1(c)). It is seen that the annealing the devices at 100 °C for 4 h results in a drastic reduction of the efficiency (0.6–2.1%). As the annealing temperature is low, the efficiency reduction cannot be attributed to the segregation and crystallization of PCBM that often takes place at temperatures >140 °C [35,36].

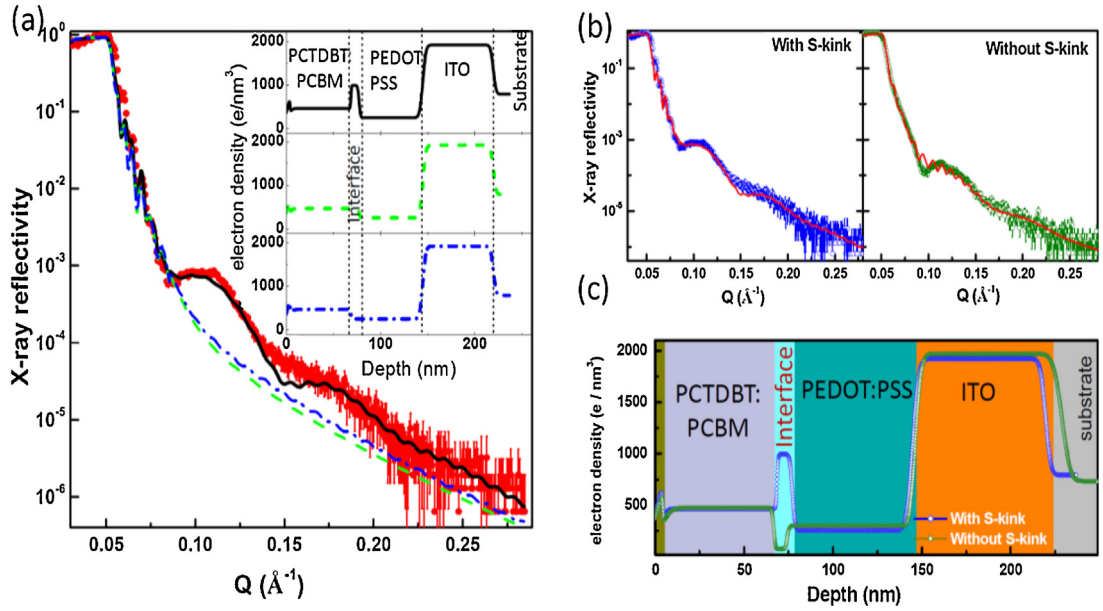

Figure 4. (a) Fitting of XRR data for a typical ITO/PEDOT:PSS/PCDTBT:PCBM/Al bulk heterojunction solar cell using different electron density profiles shown in the inset. It is seen that the best fitting is observed only when an additional interface between PCDTBT:PCBM and PEDOT:PSS is taken into account. (b) Fitting of XRR data for devices with and without S-kink in their *J–V* characteristics and (c) the resultant electron density profile.

In order to gain insight into why some of the devices show S-kink and why annealing converts diode-like behavior into S-kink behavior, we have performed XRR measurements as a function of wave vector transfer (i.e., the difference between the outgoing and incoming wave vectors), $Q = 4\pi \sin\theta/\lambda$ (where, θ is angle of incidence and λ is X-ray wavelength). In order to correlate the XRR data with *J–V* characteristics, we mimicked the BHJ solar cell by depositing only 5 nm Al layer so as to allow penetration of X-rays through the sample depth. The XRR data are qualitatively related to the Fourier transform of the electron density depth profile (EDP) $\rho(z)$ averaged over the whole sample area [36,37]. The EDP as a function of vertical depth was then inferred from the XRR data by fitting a model $\rho(z)$ whose reflectivity best fits the XRR data. A model consisted of layers included layer thickness, interface (or surface) roughness and EDP [36]. Typical experimental specular reflectivity data measured for a device as a function of wave vector transfer Q is shown in Figure 4(a). The experimental reflectivity data were fitted using the dynamical formalism of Parratt [38], as shown in the inset of Figure 4(a). By fitting the XRR data of samples without s-kink to the assumed model, we obtained the EDP profiles of various layers. However, for the samples showing the S-kink in *J–V* characteristics, the best fit of experimental data is obtained only when an additional interface of thickness ~7–9 nm was considered between PCDTBT:PCBM and PEDOT:PSS. The fitting of XRR data for the devices with and without S-kink is shown in Figure 4(b). The resultant EDP profiles across the ITO/PEDO:PSS/PCDTBT/Al was constructed from this data as shown in Figure 4(c). The thickness of the PCDTBT:PCBM layer estimated from XRR measurements is found to 70 ± 5 nm, which is equal to that of nominal thickness. Various fitting parameters of (PCDTBT:PCBM)/(PEDOT:PSS) interface are also summarized in Table 1. It is seen from the figure that EDP profiles for both samples are identical except at few nm interface of (PCDTBT:PCBM)/(PEDOT:PSS). The electron density at the (PCDTBT:PCBM)/(PEDOT:PSS) interface increases substantially from 50 to 874 e/nm^3 for devices without S-kink and with S-kink, respectively. It may be noted that the electron density obtained from XRR is total electrons in the materials i.e. Z of material (core as well as valence electrons). The EDP values obtained here are within reasonable range of values reported in literature e.g. the electron density of water obtained from XRR is 336 e/nm^3 [21] and similar values have been reported for conjugated polymers [39]. The formation of a thin high electron density layer of thickness ~7–9 nm at the interface of (PCDTBT:PCBM)/(PEDOT:PSS), for samples showing S-kink in *J–V* characteristics, could be associated with the interfacial dipoles formed as a result of chemisorbed oxygen as oxygen has high Z value. The accumulation of oxygen, as discussed above, has been confirmed by XPS measurements. The EDP values obtained here are within reasonable range of values reported in literature [39]. The formation of a thin high electron density layer of thickness ~7–9 nm at the interface between (PCDTBT:PCBM)/(PEDOT:PSS), for samples showing S-kink in *J–V* characteristics, could be associated with the interfacial dipoles form as a result of chemisorbed oxygen. It is to be noted that such a significant change in the EDP cannot result from the segregation of either PSS or PCDTBT owing to small contrast in their mass density. In addition to this, we also observed S-kink in normal devices when they were annealed at 100 °C for more than 4 h as discussed above. The EDP profiles for these samples were also constructed under abovementioned model and are shown in Figure 5. The resultant parameters of the interface are also summarized in Table 1.

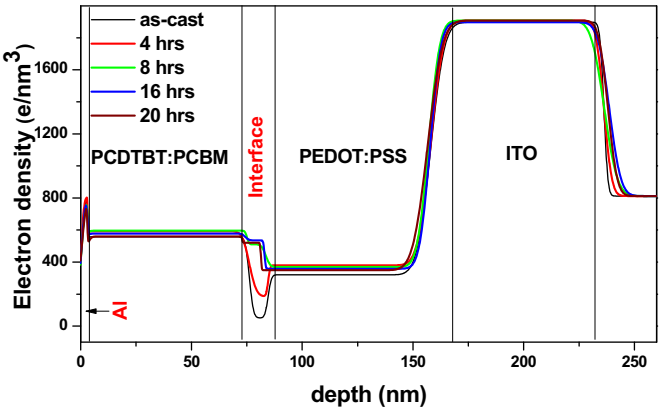

Figure 5. The electron density profile of the device with diode-like *J–V* characteristics annealed at 100 °C for different period of time. Annealing leads to increase in the electron density at the PCDTBT:PCBM/PEDOT:PSS interface as well as increase in the roughness of all the interfaces.

It is seen from the figure that annealing significantly changes the EDP profiles at the (PCDTBT:PCBM)/(PEDOT:PSS) interface. This change is observed for samples which are annealed at 100 °C for 4 h and further increment in annealing time does not change the EDP profile much. Similar kind of behavior is reflected when a drastic decrease in efficiency is observed for devices annealed at 100 °C for 4 h. In addition to this, a significant increase in the surface roughness of all the interfaces of BHJ solar cells is also observed. This is in contrast to the EDP parameters obtained for devices showing S-kink when normal devices were fabricated. Our earlier observation rule out any degradation of the donor material, i.e. PCDTBT [18]. We also rule out the segregation of PCBM as it requires high annealing temperature. The increased EDP at the (PCDTBT:PCBM)/(PEDOT:PSS) interface in this case could be attributed to segregation of PSS at 100 °C as well as diffusion of oxygen at the (PCDTBT:PCBM)/(PEDOT:PSS) interface. This may lead to roughned interfaces and S-kink observed in the *J–V* characteristics [40]. The space charge at the (PCDTBT:PCBM)/(PEDOT:PSS) interface contributes to a negative field at donor/acceptor interface, and therefore, the hole extraction is driven by diffusion against this field [5]. A competition between the diffusion and drift current (due to applied bias) is responsible for the appearance of the S-kink. The enhanced roughness of interfaces upon annealing, in addition to injection barrier, is the result of accumulation or reorganization of material at the interface.

4. Conclusions

We demonstrated a direct correlation between the electron density profile at the interface and observed S-kink in the *J–V* characteristics of the PCDTBT:PCBM based BHJ solar cells. The Kelvin Probe and XPS analyses suggest that the chemisorbed oxygen (O^{2-}) in PEDOT:PSS layer possibly modifies the structure of PCDTBT:PCBM at the interface, which results in an enhanced electron density at the interface. A correlation has been observed between the devices exhibiting high electron density at the interface and the presence of S-kink in their *J–V* characteristics upon light illumination. In addition, it was also observed that annealing of the devices causes increase in the surface roughness and increased electron density at the interfaces owing to re-organization of materials at the interface, and therefore, leads to occurrence of S-kink in devices. As the XRR is a non-destructive technique for identification of electron density profiles of multilayers, it can be utilized to predict the quality of multilayer thin-film solar cells as well as for their process optimization, especially in tandem structures.

References

[1] G. Li, R. Zhu, Y. Yang, Nat. Photonics 6 (2012) 153.
[2] B. Wu, T.Z. Oo, X. Li, X. Liu, X. Wu, E.K.L. Yeow, H.J. Fan, N. Mathews, T.C. Sum, J. Phys. Chem. C 116 (2012) 14820.
[3] R. Olivares-Amaya, C. Amador-Bedolla, J. Hachmann, S. Atahan-Evrenk, R.S. Sanchez-Carrera, L. Vogta, A. Aspuru-Guzik, Energy Environ. Sci. 4 (2011) 4849.
[4] M.O. Reese, M.S. White, G. Rumbles, D.S. Ginley, S.E. Shaheen, Appl. Phys. Lett. 92 (2008) 053307.
[5] W. Tress, K. Leo, M. Riede, Adv. Funct. Mater. 21 (2011) 2140.
[6] A. Wagenpfahl, D. Rauh, M. Binder, C. Deibel, V. Dyakonov, Phys. Rev. B 82 (2010) 115306.
[7] J. Wagner, M. Gruber, A. Wilke, Y. Tanaka, K. Topczak, A. Steindamm, U. Hörmann, A. Opitz, Y. Nakayama, H. Ishii, J. Pflaum, N. Koch, W. Brütting, J. Appl. Phys. 111 (2012) 054509.
[8] C. Falkenberg, S. Olthof, R. Rieger, M. Baumgarten, K. Muellen, K. Leo, M. Riede, Sol. Energy Mater. Sol. Cells 95 (2011) 0927.
[9] J.C. Wang, X.C. Ren, S.Q. Shi, C.W. Leung, P.K.L. Chan, Org. Electron. 12 (2011) 880.
[10] A. Kumar, S. Sista, Y. Yang, J. Appl. Phys. 105 (2009) 094512.
[11] F.A. de Castro, J. Heier, F. Nüesch, R. Hany, IEEE J. Sel. Top. Quantum Electron. 16 (2010) 1690.
[12] W. Tress, A. Petrich, M. Hummert, M. Hein, K. Leo, M. Riede, Appl. Phys. Lett. 98 (2011) 063301.
[13] Y.H. Sona, G.W. Kima, W.S. Jeona, R. Podeb, J.H. Kwona, Mol. Cryst. Liq. Cryst. 565 (1) (2012) 8.
[14] G.K. Mor, T.P. Le, K. Vakhshouri, D.R. Kozub, E.D. Gomez, ACS Appl. Mater. Interfaces 6 (22) (2014) 19638.
[15] Q. Yang, J. Wang, X. Zhang, J. Zhang, Y. Fu, Z. Xie, Sci. China Chem. 58 (2015) 309.
[16] W. Tress, S. Corvers, K. Leo, M. Riede, Adv. Energy Mater. 3 (2013) 873.
[17] W. Tress, O. Inganäs, Sol. Energy Mater. Sol. Cells 117 (2013) 599.
[18] A. Gusain, V. Saxena, P. Veerender, P. Jha, S.P. Koiry, A.K. Chauhan, D.K. Aswal, S.K. Gupta, AIP Conf. Proc. 776 (2013) 1512.
[19] Z. Li, H.C. Wong, Z. Huang, H. Zhong, C.H. Tan, W.C. Tsoi, J.S. Kim, J.R. Durrant, J.T. Cabral, Nat. Commun. 4 (2013) 2227.
[20] M.R. Fitzsimmons, C. Majkrzak, Modern Techniques for Characterizing Magnetic Materials, Springer, New York, 2005, pp. 107 (Chapter 3).
[21] G. Luo, W. Bu, M. Mihaylov, I. Kuzmenko, M.L. Schlossman, L. Soderholm, J. Phys. Chem. C 117 (2013) 19082.
[22] S. Wakim, S. Beaupr, N. Blouin, B.R. Aich, S. Rodman, R. Gaudiana, Ye. Tao, M. Leclerc, J. Mater. Chem. 19 (2009) 5351.
[23] J.W. Kingsley, P.P. Marchisio, H. Yi, A. Iraqi, C.J. Kinane, S. Langridge, R.L. Thompson, A.J. Cadby, A.J. Pearson, D.G. Lidzey, R.A.L. Jones, A.J. Parnell, Sci. Rep. 4 (2014) 5286.
[24] S.H. Park, A. Roy, S. Beaupre, S. Cho, N. Coates, J.S. Moon, D. Moses, M. Leclerc, K. Lee, A.J. Heeger, Nat. Photonics 3 (2009) 297.
[25] B. Kim, H.R. Yeom, M.H. Yun, J.Y. Kim, C. Yang, Macromolecules 45 (2012) 8658.
[26] E.A. Parlak, T.A. Tumay, N. Tore, S. Sarıoğlan, P. Kavak, F. Turksoy, Sol. Energy Mater. Sol. Cells 110 (2013) 58.
[27] F. Etzold, I.A. Howard, R. Mauer, M. Meister, T.D. Kim, K.W. Lee, N.S. Back, F. Laquai, J. Am. Chem. Soc. 133 (2011) 9469.
[28] N. Koch, A. Elschner, J. Schwartz, A. Kahn, Appl. Phys. Lett. 82 (2003) 2281.
[29] N. Koch, A. Elschner, J.P. Rabe, R.L. Johnson, Adv. Mater. 17 (2005) 330.
[30] F. Petraki, S. Kennou, S. Nespurek, J. Appl. Phys. 103 (2008) 033710.
[31] G. Greczynski, Th. Kugler, W.R. Salaneck, Thin Solid Films 354 (1999) 129.
[32] K. Fehse, R. Meerheim, K. Walzer, K. Leo, W. Lövenich, A. Elschner, Appl. Phys. Lett. 93 (2008) 083303.
[33] K. Norrman, M.V. Madsen, S.A. Gevorgyan, F.C. Krebs, J. Am. Chem. Soc. 132 (2010) 16883.
[34] T. Nagata, S. Oh, T. Chikyow, Y. Wakayama, Org. Electron. 12 (2011) 279.
[35] J.W. Kiel, B.J. Kirby, C.F. Majkrzak, B.B. Maranville, M.E. Mackay, Soft Matter 6 (2010) 641.
[36] Y. Xie, Y. Bao, J. Du, C. Jiang, Q. Qiao, Phys. Chem. Chem. Phys. 29 (2012) 10168.
[37] S. Singh, M.R. Fitzsimmons, T. Lookman, J.D. Thompson, H. Jeen, A. Biswas, M.A. Roldan, M. Varela, Phys. Rev. Lett. 108 (2012) 077207.
[38] L.G. Parratt, Phys. Rev. 95 (1954) 359.
[39] Y.G. Ko, W.D. Kwon, M. Kim, K. Kim, Y.S. Gal, M. Ree, Polym. Chem. 3 (2012) 2028.
[40] F.C. Krebs, K. Norrman, Prog. Photovolt.: Res. Appl. 15 (2007) 697.